

# Spectral analysis in orbital/superorbital phase space and hints of superorbital variability in the hard X-rays of LS I +61°303

Jian Li<sup>1</sup>, Diego F. Torres<sup>1,2</sup>, & Shu Zhang<sup>3</sup>

## ABSTRACT

We present INTEGRAL spectral analysis in the orbital/superorbital phase space of LS I +61°303. A hard X-ray spectrum with no cutoff is observed at all orbital/superorbital phases. The hard X-ray index is found to be uncorrelated with the radio index (non-simultaneously) measured at the same orbital and superorbital phases. In particular, the absence of an X-ray spectrum softening during the periods of negative radio index does not favor a simple interpretation of the radio index variations in terms of changes of state in a microquasar. We uncover hints for the superorbital variability in the hard X-ray flux, in phase with the superorbital modulation in soft X-rays. An orbital phase drift of radio peak flux and index along the superorbital period is observed in the radio data. We explore its influence on a previously reported double peak structure of radio orbital lightcurve, posing it as a plausible explanation.

*Subject headings:* X-rays: observations, X-ray binaries: individual (LS I +61°303)

## 1. Introduction

LS I +61°303 is a high mass X-ray binary hosting a B0 Ve star with an equatorial outflowing disk. The companion is orbited by a compact object with an orbital period of 26.496 days (e.g., Casares et al. 2005). LS I +61°303 is detected up to GeV and TeV gamma-rays (Albert et al. 2006; Abdo et al. 2009; Acciari et al. 2009; Hadasch et al. 2012), and the non-thermal spectral energy distribution is dominated by high energy photons. Two short ( $< 0.1$  s) and highly luminous ( $> 10^{37}$  erg s<sup>-1</sup>) thermal flares were detected recently from the direction of LS I +61°303 (Barthelmy et al. 2008; Burrows et al. 2012), giving

---

<sup>1</sup>Institute of Space Sciences (IEEC-CSIC), Campus UAB, Torre C5, 2a planta, 08193 Barcelona, Spain

<sup>2</sup>Institució Catalana de Recerca i Estudis Avançats (ICREA).

<sup>3</sup>Laboratory for Particle Astrophysics, Institute of High Energy Physics, Beijing 100049, China.

support to the hypothesis that the compact object in LS I +61°303 is a (at least internally) highly magnetized neutron star (Torres et al. 2012; Papitto et al. 2012).

Besides the orbital period of 26.496 days, and other short-timescale variability (see e.g., Paredes et al. 2007), LS I +61°303 is known to have a long-term (1667 days) superorbital modulation. The latter was first discovered in radio (Paredes 1987; Gregory 1989; Gregory 1999; Gregory 2002), and then observed in H $\alpha$  emission line (Zamanov et al. 1999), X-rays (Li et al. 2012; Chernyakova et al. 2012), GeV (Ackermann et al. 2013), and hinted at TeV (Li et al. 2012; Torres et al. 2012). The possible origin of this 1667 days superorbital modulation could be the precession of the Be disk (Lipunov & Nazin 1994), the beat frequency between the orbital and precessional rates in a microquasar scenario (Massi & Jaron 2013), or the cyclic variability in the Be star envelope. The last interpretation seems the most natural, since the H $\alpha$  emission line varies on the same period and it is well known for the Be stars that the size of the circumstellar disk grows as the equivalent width of H $\alpha$  increases (e.g., Hanushik, Kozok & Kaizer, 1988). In the maximum of the equivalent width of H $\alpha$ , the X-ray as well as  $\gamma$ -ray emission are enhanced (Li et al. 2012; Ackermann et al. 2013). The orbital phase of the X-ray peaks from LS I +61°303 varies from 0.35 to 0.75 along the superorbital period, consistently leading the radio peaks by 0.2 orbital phase (Chernyakova et al. 2012). The different origin regions of X-ray and radio emission could lead to the observed phase lag. The observed multiwavelength variabilities in superorbital timescale were discussed in the scenario of a neutron star switching between ejector and propeller states by Torres et al. (2012) and Papitto et al. (2012).

Black hole composed microquasars manifest themselves in five classical spectral X-ray states (van der Klis 1994; Tanaka & Lewin 1995; Tanaka & Shibazaki 1996; Esin et al. 1997): the high/soft (HS) state, the low/hard (LH) state, the quiescent state, the very high (VH) state, and the intermediate state. These spectral states were regrouped by McClintock & Remillard (2006) as thermal–dominant (TD), hard X-ray, quiescent, steep powerlaw (SPL), and intermediate states. From an observational perspective, an optically thick steady jet with flat (radio spectral index  $\alpha \sim 0$ ) or inverted ( $\alpha \geq 0$ ) radio component is usually seen when in the hard X-ray state (a power law spectrum with index  $1.5 < \Gamma < 2.1$  in X-rays, McClintock & Remillard 2006), and an optically thin transient jet ( $\alpha < 0$ ) is associated with the overall hard to soft state transition (Fender et al. 2004; Fender et al. 2009).

In the hypothesis of LS I +61°303 being a microquasar, the explanation for the short thermal flares that have been detected from the region of LS I +61°303 must be the spatial superposition of a magnetar with a gamma-ray binary, however unlikely. In this hypothesis, Zimmermann & Massi (2012) expected a steady jet ( $\alpha \geq 0$ ) in the hard X-ray state of the source, thus characterized by a power law with index  $1.5 < \Gamma < 1.8$  and a cutoff at

high energies. A transient jet (with  $\alpha < 0$ ) would on the contrary be expected in the SPL state of LS I +61°303, showing an X-ray slope of  $\Gamma \geq 2.4$ . These seem very simplified assumptions, given that such an SPL state is poorly characterized. McClintock & Remillard (2006) note that many BH binaries could be radio quiet during this phase, and moreover, such state seems often described by high X-ray luminosity ( $> 0.2$  times the Eddington level) and the detection of a thermal component or QPOs; all of which are clearly not the case of LS I +61°303 (Li et al. 2011).

Although GBI radio data showed spectral index transitions (Massi & Kaufman Bernadó, 2009), the photon index of INTEGRAL observations was found to be compatible with a low hard state (Chernyakova et al. 2006; Zhang et al. 2010) at all times. Only in one occasion the photon index was  $\Gamma = 3.6^{+1.6}_{-1.1}$  (Chernyakova et al. 2006). However, the large error bars (due to little exposure) introduced a large uncertainty. Zimmermann & Massi (2012) demonstrated that averaging the INTEGRAL data over too large orbital and superorbital phase ranges can result in a dominant low hard state and smear out the SPL state. This effect, they posed, is what explains the hard spectra all along the orbit in the LS I +61°303 system, and which led to the inconsistency between data and their predictions. Here, using INTEGRAL observations that double the size of our previous analysis (Zhang et al. 2010) and two years more data than in Chernyakova et al. (2012) we can separate in orbital and superorbital phases and test these ideas.

## 2. Observations and data analysis

INTEGRAL (Winkler et al. 2003) is a  $\gamma$ -ray mission covering the energy the range 15 keV–10 MeV. Observations are carried out in individual Science Windows (ScW), which have a typical time duration of about 2000 s. We use all public IBIS/ISGRI data for which LS I +61°303 has an offset angle less than 14°. Our data set comprises about 2006 ScWs. The data cover revolutions 6–1317, from 2002-11-01 to 2013-07-27 (MJD 52579–56500), adding up to a total effective exposure time of 928 ks in IBIS/ISGRI. The data reduction is performed using the standard ISDC offline scientific analysis (OSA 10.0). IBIS/ISGRI images for each ScW are generated in the energy band of 18–60 keV. The count rate at the position of the source are extracted from all individual images to produce the long-term lightcurve on the ScW timescale. The spectra of LS I +61°303 are produced for each of the ScW following the standard steps as stated in the IBIS Analysis User Manual, running the pipeline from the raw data to SPE level<sup>1</sup>. All of the spectral analysis is performed using XSPEC 12.8.1;

---

<sup>1</sup>Please see <http://www.isdc.unige.ch/integral/analysis> for more information

uncertainties are given at the  $1\sigma$  confidence level for one single parameter of interest.

We have also considered radio data from NASA/NRAO Green Bank Interferometer (GBI) database. The radio data set, the same as the one used by Massi & Kaufman Bernadó (2009) and Zimmermann & Massi (2012), covers LS I +61°303 at  $\nu_1 = 2.25$  GHz and  $\nu_2 = 8.3$  GHz for 6.7 years in three periods of MJD 49379.975–50174.710, MJD 50410.044–51664.879 and MJD 51798.333–51823.441. The radio spectral index  $\alpha$  and its error  $\Delta\alpha$  are calculated as  $\alpha = \frac{\log(S_1/S_2)}{\log(\nu_1/\nu_2)}$  and  $\Delta\alpha = \frac{0.434}{\log(\nu_1/\nu_2)} \sqrt{(\frac{\Delta S_1}{S_1})^2 + (\frac{\Delta S_2}{S_2})^2}$ , where  $S_{1,2}$  are the corresponding radio fluxes at the two frequencies of interest.

### 3. Results

#### 3.1. INTEGRAL spectral analysis in the orbital/superorbital phase space

The orbital phase of an X-ray binary system represents a unique location of the compact object in the orbit. The compact object will encounter a similar physical environment (e.g. magnetic field, mass density, accretion rate, etc.) in the same orbital phase if the properties of companion star are stable, which will presumably lead to a repetitive pattern of orbital emissions.

Long-term stability of the X-ray orbital lightcurve is observed in LS 5039 (Kishishita et al. 2009). Unlike LS 5039, hosting an O star with a relative stable stellar wind, LS I +61°303’s companion is a Be star with circumstellar disk variability, which presumably gives rise to the superorbital period. Because of the different configuration of the circumstellar disk along the superorbital period, the physical environment in each orbit is different even for the same orbital phase. Consequently, we observe variable orbital emission from LS I +61°303 along the superorbital period in all frequencies (Paredes 1987; Gregory 1989; Torres et al. 2010; Li et al. 2012; Chernyakova et al. 2012; Ackermann et al. 2013). Averaging data over too large orbital and superorbital phase ranges mixes different physical conditions and smears out information (Zimmermann & Massi 2012). In order to expect a similar physical configuration in the LS I +61°303 system, one should then require not only a similar orbital phase, but also a similar superorbital phase.

With all INTEGRAL data combined, LS I +61°303 is detected with a significance of  $10.59\sigma$  in the 18–60 keV band (Fig. 1, left panel). INTEGRAL hard X-rays and GBI radio data distribution in the orbital/superorbital phase space are shown in Fig. 2, left panels. This is similar to Fig. 4 in Gregory 2002 and Fig. 2 in Chernyakova et al. 2012 for their respective datasets. The number of observations at each position in the phase space is given

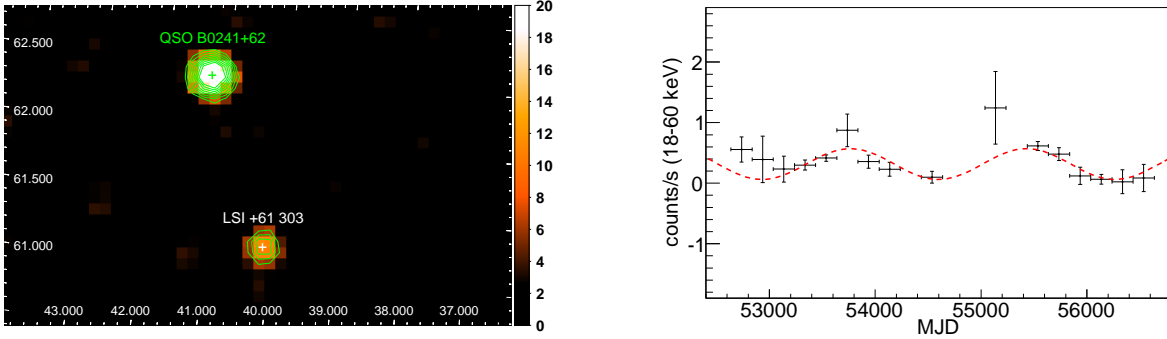


Fig. 1.— Left panel: mosaic image of the LS I +61°303 sky region, derived by combining all INTEGRAL/ISGRI data. The brighter source is QSO 0241+622 (at the upper part of the image) and the relatively faint one is LS I +61°303. Corresponding significances and color can be found in the right color bar. The contours start at a detection significance level of  $6\sigma$ , with each step being  $2\sigma$ . The X- and Y-axes are R.A. and decl. in units of degrees. Right panel: long-term lightcurve of LS I +61°303 in 18-60 keV binned in 200 days. The dotted red line indicates a sinusoidal fitting with the superorbital period fixed.

by the color scale. Although the radio (MJD 49379.975–51823.441) and hard X-ray data (MJD 52579–56500) do not overlap in time, some are co-located at the same orbital and superorbital phases. Fig. 2, upper right panel, shows the overlapped INTEGRAL and GBI observations in phase space. The radio index for the phase space when hard X-rays and radio observations are both available (Fig. 2, left panels) is shown in the bottom right panel of the same figure (light blue stands for  $\alpha < 0$ ; dark blue stands for  $\alpha > 0$ ).

LS I +61°303 should be in SPL state/low hard state with photon index  $\Gamma > 2.4$  and  $1.5 < \Gamma < 1.8$  respectively according to Zimmermann & Massi (2012). To test this, we have extracted the INTEGRAL spectra in the expected SPL state ( $\alpha < 0$ , light blue region) and low hard state ( $\alpha > 0$ , dark blue region), respectively. X-ray spectra are well fitted with a simple power-law without high energy cutoffs. The results are shown in Table 1. The X-ray photon index is hard ( $\Gamma = 1.49^{+0.21}_{-0.19}$ ) when the radio index  $\alpha < 0$ , what happens for most of the observations. This is not consistent with the predictions mentioned. In the case of radio index  $\alpha > 0$ , the X-ray photon index results in  $\Gamma = 2.59^{+1.01}_{-0.83}$ . The large error bars are expected from the much less effective exposure (see Table 1). Because of the large uncertainty, no significant difference could be drawn between the two X-ray spectra.

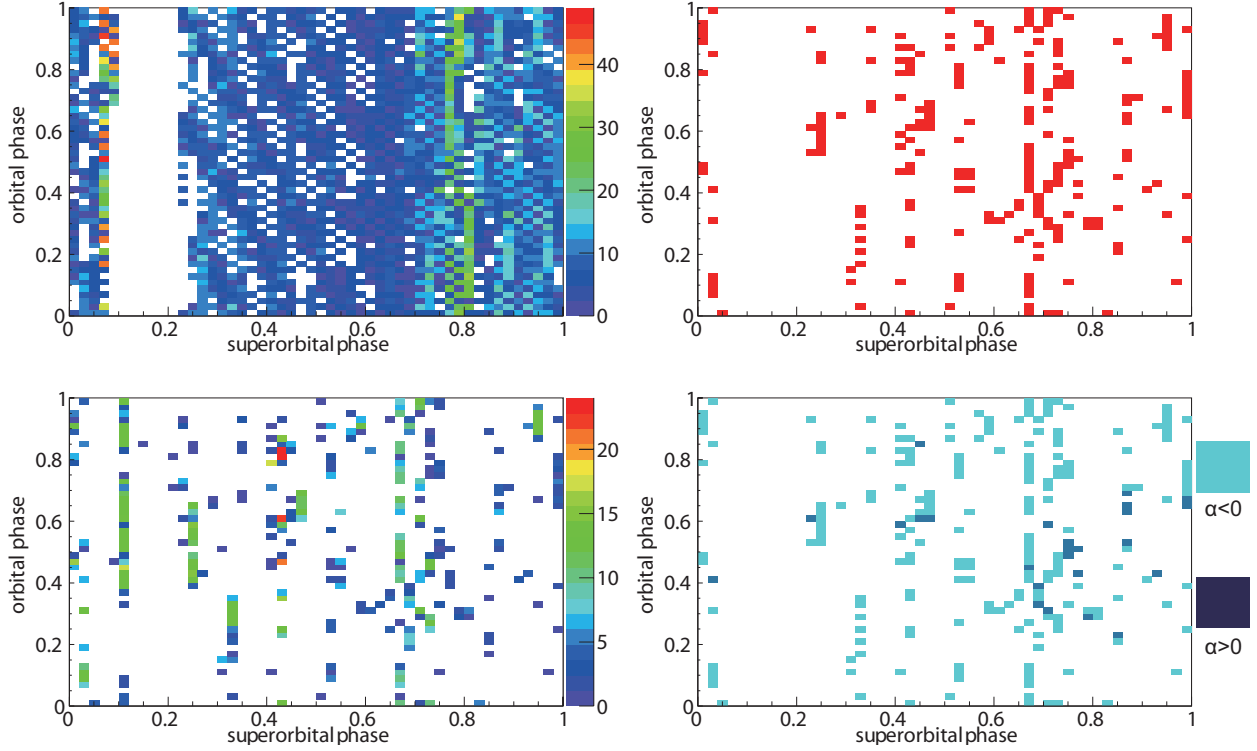


Fig. 2.— GBI (upper left) and INTEGRAL (bottom left) data distribution in orbital/superorbital phase space. The number of observations are given by the color scale. The upper right panel shows the part of the phase space with overlapped GBI and INTEGRAL observations. The radio index of overlapped INTEGRAL and GBI observations are shown in the bottom right panel (light blue stands for  $\alpha < 0$ ; dark blue stands for  $\alpha > 0$ ).

### 3.2. Hints of superorbital variability of LS I +61°303 in hard X-ray

The INTEGRAL observations cover LS I +61°303 for more than 10 years. The long-term lightcurve in the 18–60 keV band binned in 200 days is shown in Fig. 1, right panel. A constant fit to the lightcurve yields an average flux of  $0.34 \pm 0.03$  counts/s and a reduced  $\chi^2$  of 50.92/16, which indicates variability at the  $4.3 \sigma$  level. The lightcurve can be fitted by a sinusoidal function with fixed period at 1667 days, yielding a reduced  $\chi^2$  of 13.42/14 (Fig. 1, right panel). An F-test shows that the possibility of wrongly refusing the sinusoid is  $8.83 \times 10^{-5}$ .

We fold the INTEGRAL ScW lightcurve at 1667 days superorbital period with  $T_0$  at MJD 43366.275. A clear modulation profile is seen (Fig. 3, left top panel). A constant fit to the lightcurve yields a reduced  $\chi^2$  of 36.8/7, indicating variability at  $4.6 \sigma$  level. The

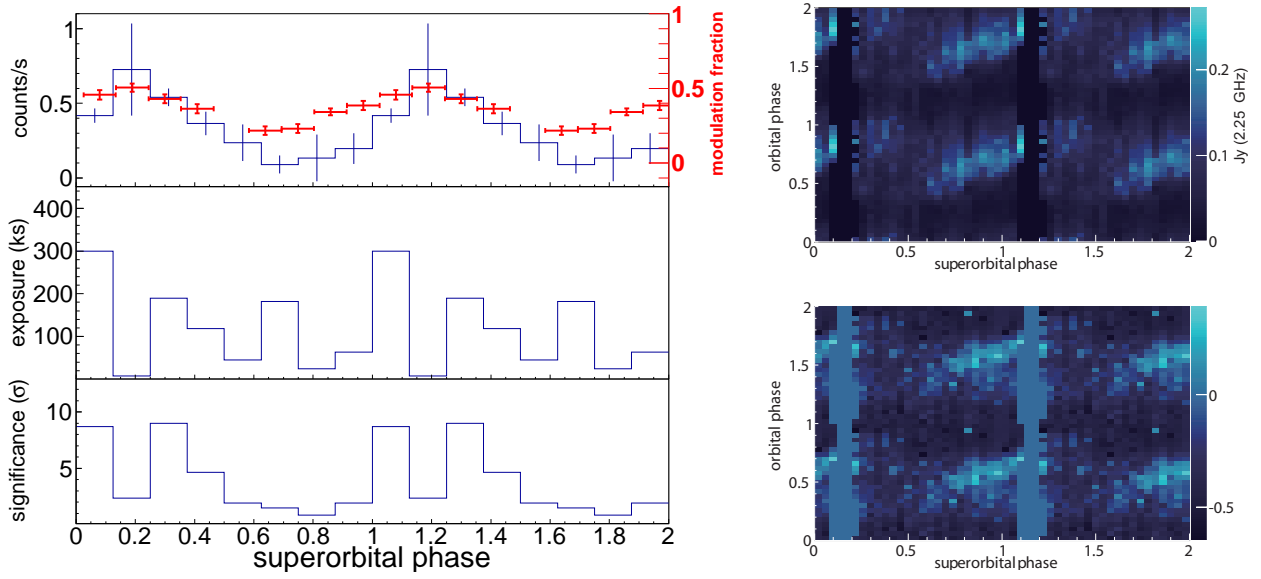


Fig. 3.— Left: Superorbital lightcurve of LS I +61°303 in the 18–60 keV, as observed by INTEGRAL. The red points show the modulated fraction in the 3–30 keV band, from Li et al. 2012. Middle and bottom: exposure and significance for the corresponding superorbital phase, respectively. Right: radio flux intensity at 2.25 GHz (top) and spectral index (bottom) as a function of the orbital and superorbital phases.

superorbital lightcurve of LS I +61°303 in hard X-rays peaks around superorbital phase  $\sim 0.2$ , which is in phase with superorbital modulation in soft X-ray (the red points in Fig. 3, left top panel, showing the modulated fraction in the 3–30 keV band, from Li et al. 2012). Exposure time and significance of corresponding superorbital phase are shown in Fig. 3 (left), middle and bottom panels. The large error bar of the superorbital lightcurve peak happens as a result of the low exposure time ( $\sim 7.4$  ks) it has compared to other phases (hundreds ks). We extract spectra for different superorbital and orbital phases. All spectra are well fitted by a simple powerlaw. The fitting parameters are shown in Table 1.

### 3.3. Orbital phase drift of the radio peak flux and index

In X-ray and radio bands, the superorbital modulation manifest itself not only in the peak flux or the modulated fraction variation (Gregory 2002; Li et al. 2012), but also in a systematic drift of the orbital phase of peak flux and spectral index (Ray et al. 1997; Gregory 2002; Chernyakova et al. 2012). We have detected the drift of the peak flux and spectral index in radio data, consistent with the results in Gregory (2002) and Chernyakova et al.



(2012). From superorbital phase  $\sim 0.6$  to  $\sim 1.5$ , the orbital phase of the radio peak flux (both 2.25 GHz and 8.3 GHz data show a similar evolution, see Fig. 3) is linearly drifting from orbital phase  $\sim 0.5$  to  $\sim 0.95$ . The linear drift of the spectral index is less evident, but clearly shifted earlier –by  $\sim 0.1$  in orbital phase– compared to the flux (Fig 3, right bottom panel). Because of the scarce orbital coverage of INTEGRAL along the superorbital period (Fig. 2, bottom left panel), we are unable to explore the presence of a peak flux drift in hard X-rays yet.

Massi & Kaufman Bernadó (2009) claimed that the periodic radio orbital outbursts consisted of two peaks. We pose here that the two-peak structure is related to the drift of radio peak flux along the superorbital period. Fig. 3 of Massi & Kaufman Bernadó (2009) shows the radio orbital lightcurve during superorbital phase 0.0–0.1, in which the authors claimed two peaks at orbital phase 0.69 and 0.82. But in our Fig. 3, right top panel, it is clear that the orbital phase of radio peaks drifts from  $\sim 0.7$  to  $\sim 0.8$  during superorbital phase 0.0–0.1. Thus, to explore drifts in detail, we display the lightcurves of 2.25 GHz (top panel), 8.3 GHz (middle panel) and the radio index (bottom panel) during superorbital phase 0.0–0.1 in Fig. 4, where each orbit is noted with a different color. The radio data cover more than one superorbital period, from superorbital phases  $\sim 3.6$  to  $\sim 5.1$ ; the data in the superorbitally folded bin 0.0–0.1 was gathered in two passages corresponding to superorbital phase 4.0–4.1 and 5.0–5.1. These results are shown in Fig. 4. In the right panel of Fig. 4 we show the corresponding folded orbital lightcurve in superorbital phase 0.0–0.1, similarly to Fig. 3 of Massi & Kaufman Bernadó (2009), but keeping the different color for the different orbits. The phases of the reported two peaks (Massi & Kaufman Bernadó 2009) are indicated with dashed black lines. In Fig. 4, right top and middle panel, it is apparent to the eye that the phase of peak flux in 2.25 GHz and 8.3 GHz is drifting in each orbit. The orbital lightcurve depicted in green is peaking around orbital phase  $\sim 0.69$ , which is the first peak reported in Massi & Kaufman Bernadó (2009), while several orbits later, the black-colored lightcurve is peaking at orbital phase  $\sim 0.82$ , which is near the second peak reported. Thus, folded in superorbital phase (0.0–0.1), the two peaks in Fig. 3 of Massi & Kaufman Bernadó (2009) may actually be a superposition of single peaks from different orbits. Similarly, this orbital peak drifting may also have effects in Fig. 5 of Massi & Kaufman Bernadó (2009), where the data is also folded over a bin of 0.1 superorbital phase. Thus, only the lightcurve of each individual orbit, or the orbital lightcurve folded in a narrower superorbital phase that avoids the orbital peak-drifting effect is suitable to explore the reality of the double peak structure, which is here put in question.



#### 4. Discussion

We have tested one of the methods proposed to identify the microquasar nature of the LS I +61°303 system: Namely, that it is in SPL state when the radio index  $\alpha < 0$  and in low hard state when  $\alpha > 0$ , and that using large orbital and superorbital phase ranges mixes these states smearing out the state transitions signatures (Zimmermann & Massi 2012). The latter has been claimed as the reason of the non-detection of significant spectral variations in the INTEGRAL data analyzed so far. Here, with a significantly increased dataset, we have introduced the orbital / superorbital phase space and extracted the X-ray spectrum for the corresponding specific cuts, avoiding averaging data over a too large superorbital range. LS I +61°303 shows a hard spectrum (single power law with no cutoff,  $\Gamma=1.49_{-0.19}^{+0.21}$ , see Table 1) when  $\alpha < 0$ , which is inconsistent with the SPL state interpretation of Zimmermann & Massi (2012) stated above.

As commented in the introduction, such a clear cut distinction between states based on the radio index seems unlikely. The SPL state itself is not an “intermediate state” that lies between soft and hard states, though transitions pass through SPL frequently (McClintock & Remillard 2006; Zhang et al. 2013). It may also be unrealistic to think that optically thin radio emission is confined to the SPL state only. If a hard to soft state transition does not pass through an SPL state (e.g., the 2011 outburst of H 1743-322 during which the photon index is always below 2.4, Zhou et al. 2012) or optically thin radio flares appear in other intermediate states but not in SPL state, the X-ray photon index will not go above 2.4 during optically thin radio emission. Thus, the X-ray spectrum during  $\alpha < 0$  might be a mixture of a SPL state or transitions to SPL states (e.g. see the cases of XTE J1650-500, Corbel et al. 2004; GX 339-4, Gallo et al. 2004; XTE J1859+226, Brocksopp et al. 2002, Corbel et al. 2004), and intermediate states when optically thin radio emissions locate out of SPL states. Nevertheless, the fact that most of the observation time in INTEGRAL indeed has a concurrent  $\alpha < 0$  (at the same orbital and superorbital phase) indicates that the most likely alternative is simply that there is no state transition at all, something also supported by the low X-ray flux at all times.

We have also shown hints for the superorbital variability of LS I +61°303 in hard X-rays, and that the appearance of a double peak structure in the radio lightcurve of superorbitally folded data can be accommodated by a drift of a single peak in an orbital basis.

We acknowledge the grants AYA2012-39303, as SGR2009-811, iLINK2011-0303, NSFC 11073021, 11133002, 11103020, XTP project XDA04060604 and the Strategic Priority Research Program “The Emergence of Cosmological Structures” of the Chinese Academy of Sciences, grant No. XDB09000000. JL acknowledges support by the Faculty of the European

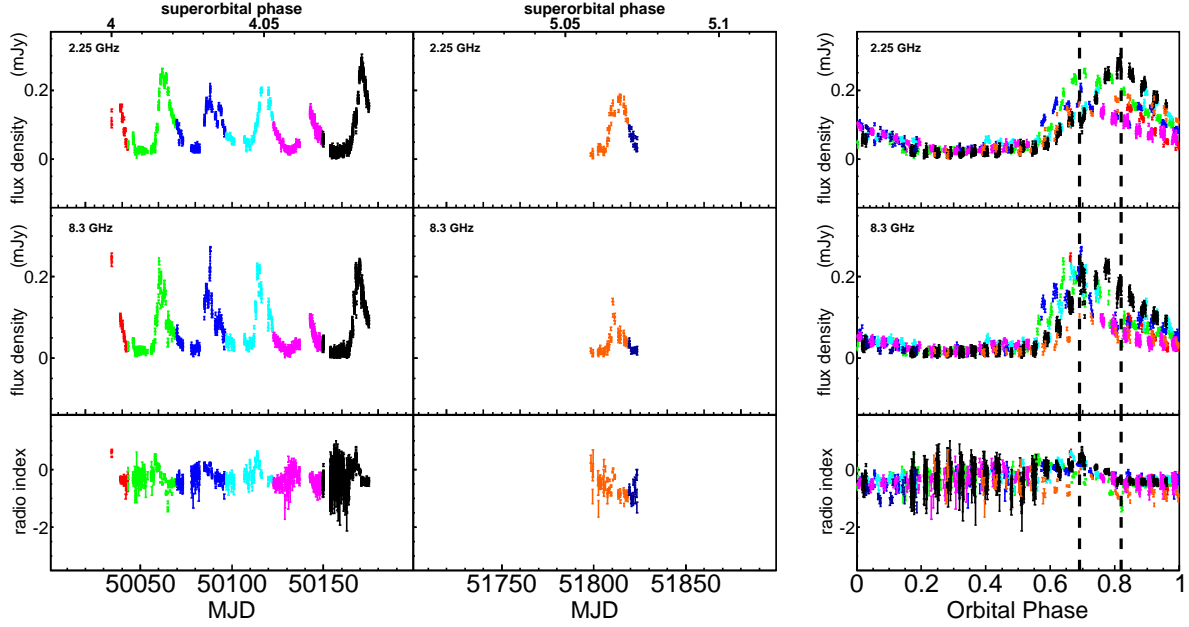


Fig. 4.— Left and Middle Panel: lightcurves of 2.25 GHz (top panel), 8.3 GHz (middle panel) and radio index (bottom panel) during superorbital phase 0.0–0.1. Superorbital phase is shown as the upper axis on top of the panels. Right Panel: folded orbital lightcurve of 2.25 GHz (top panel), 8.3 GHz (middle panel) and radio index (bottom panel) during superorbital phase 0.0–0.1. The two peaks reported in Massi & Kaufman Bernadó 2009 are shown with dashed black lines. Different orbit (orbital phase 0.0–1.0) are shown with different color.

Space Astronomy Centre. DFT further acknowledges the Chinese Academy of Sciences visiting professorship program 2013T2J0007. We thank M. Massi for facilitating us her collected radio data and A. Papitto & N. Rea for comments.

## REFERENCES

- Abdo et al. 2009, *ApJ*, 701, 123
- Acciari, V. A., Aliu, E., Arlen, T., et al. 2009, *ApJ*, 700, 1034
- Ackermann M. et al., 2012, *Science*, 335, 189
- Ackermann M. et al., 2013, *ApJ*, 773, 35
- Albert, J., Aliu, E., Anderhub, H., et al. 2006, *Science*, 312, 1771
- Barthelmy, S. D., Baumgartner, W., Cummings, J., et al. 2008, *GCN Circ.*, 8215, 1

- Burrows, D. N., Chester, M. M., DElia, V., et al. 2012, GCN Circ., 12914, 1
- Brocksoopp, C., et al. 2002, MNRAS, 331, 765
- Casares, J., Ribas, I., Paredes, J. M., Martí J., Allende, P. C., 2005, MNRAS, 360, 1105
- Corbel, S., Fender, R. P., Tomsick, J. A., Tzioumis, A. K. & Tingay, S., 2004, ApJ, 617,1272
- Chernyakova, M., Neronov, A., & Walter, R. 2006, MNRAS, 372, 1585
- Chernyakova, M. , Neronov, A., Molkov, S., Malyshev, D.,Lutovinov, A.& Pooley G.2012, ApJ, 747, 29
- Esin, A.A., McClintock, J.E. & Narayan, R. 1997, ApJ 489, 865
- Fender, R. P., Belloni, T. M., & Gallo, E. 2004, MNRAS, 355, 1105
- Fender, R. P.,Homan, & J Belloni. 2009, MNRAS, 396, 1370
- Gallo, E., Corbel, S., Fender, R. P., Maccarone, T. J. & Tzioumis, A. K., 2004, MNRAS, 347,52
- Gregory, P.C, Xu, Huang-jian, Backhouse C.J., Reid, A., 1989, ApJ, 339, 1054
- Gregory, P.C, 1999, ApJ, 520,361
- Gregory, P. C. 2002, ApJ, 575, 427
- Hadasch, D., Torres, D. F., Tanaka, T., et al. 2012, ApJ 749, 54
- Kishishita, T., Tanaka, T., Uchiyama, Y., Takahashi, T. et al. 2009, ApJ, 697, 1
- Li, J., Torres, D. F., Zhang, S., et al. 2011, ApJ 733, 89
- Li, J., Torres, D. F., Zhang, S., et al. 2012, ApJ 744, 13
- Lipunov, V. M., & Nazin, S. N. 1994, A&A, 289, 822
- Massi, M., & Kaufman Bernadó, M. 2009, ApJ, 702, 1179
- Massi, M. & Jaron F. 2013, A&A, 554, 105
- McClintock, J. E., & Remillard, R. A. 2006, in Compact Stellar X-ray Sources, ed. W. Lewin & M. van der Klis (Cambridge: Cambridge Univ. Press), 157 (arXiv:0306213)
- Papitto, A., Torres, D. F., & Rea N. 2012, ApJ 756, 188

- Paredes, J.M, 1987, PhD Thesis, University of Barcelona
- Paredes, J.M, et al. 2007, ApJ Letters, 664, 39
- Ray, et al. 1997, ApJ 491, 381
- Rea, N., Torres, D. F., van derKlis, M., Jonker, P. G., Méndez, M. & Sierpowska-Bartosik, A. 2010, MNRAS, 405, 2206
- Tanaka, Y. and Lewin, W.H.G. (1995), in X-ray Binaries, eds. W.H.G. Lewin, J. van Paradijs and E.P.J. van den Heuvel, (Cambridge U. Press, Cambridge) 126-174, TL95
- Tanaka, Y. and Shibazaki, N. (1996), ARA&A 34, 607-644, TS96
- Torres, D. F., Rea, N., Esposito, P., et al. 2012, ApJ 744, 106
- van der Klis, M. (1994), ApJS 92, 511-519
- Winkler, C. et al., 2003, A&A, 411, L1
- Zamanov, R. & Marti, J., 1999, A&A, 358, 55
- Zhang, S, Torres, D. F., Li, J. et al. 2010, MNRAS, 408, 642
- Zhang, S-N, 2013, Invited review article in a special issue of the journal "Frontiers of Physics", dedicated to the topic of "High energy astrophysics". Eds. Bing Zhang & Péter Mészáros (arXiv:1302.5485)
- Zhou, J.N. et al. 2013, MNRAS, 431, 2285
- Zimmermann, L. & Massi M. 2012, A&A, 537, 82

Table 1: X-ray spectra parameters associated with observations providing a radio index  $\alpha < 0$  and  $\alpha > 0$  and superorbitally / orbitally separated spectra from INTEGRAL/ISGRI observations.

Radio index	X-ray photon index $\Gamma$	Flux (18–60 keV) $10^{-11} \text{ erg cm}^{-2} \text{ s}^{-1}$	Reduced $\chi^2(D.O.F)$	Effective exposure ks
$\alpha < 0$	$1.49^{+0.21}_{-0.19}$	$1.67 \pm 0.19$	0.86 (4)	508.0
$\alpha > 0$	$2.59^{+1.01}_{-0.83}$	$2.10^{+0.58}_{-0.59}$	0.57 (5)	42.8
Superorbital phase	X-ray photon index $\Gamma$	Flux (18–60 keV) $10^{-11} \text{ erg cm}^{-2} \text{ s}^{-1}$	Reduced $\chi^2(D.O.F)$	Effective exposure ks
0.1–0.2	$1.06^{+0.22}_{-0.23}$	$2.14 \pm 0.23$	0.254 (5)	238.9
0.2–0.3	$1.79^{+0.23}_{-0.21}$	$3.65 \pm 0.36$	0.330 (7)	133.1
0.3–0.5	$1.66^{+0.31}_{-0.28}$	$1.87 \pm 0.29$	1.00 (4)	182.3
0.5–0.8	$1.27^{+0.40}_{-0.38}$	$1.31 \pm 0.29$	0.975 (3)	241.0
0.8–1.1	$1.27^{+0.44}_{-0.39}$	$1.52^{+0.42}_{-0.40}$	0.688 (4)	134.4
Orbital phase	X-ray photon index $\Gamma$	Flux (18–60 keV) $10^{-11} \text{ erg cm}^{-2} \text{ s}^{-1}$	Reduced $\chi^2(D.O.F)$	Effective exposure ks
0.0–0.4	$1.90^{+0.47}_{-0.40}$	$1.63 \pm 0.29$	0.256 (4)	219.3
0.4–0.5	$1.60^{+0.22}_{-0.21}$	$2.84 \pm 0.30$	0.763 (5)	162.3
0.5–0.6	$1.54^{+0.28}_{-0.25}$	$2.84 \pm 0.39$	0.358 (8)	118.2
0.6–0.7	$1.44^{+0.32}_{-0.30}$	$2.24 \pm 0.35$	0.424 (4)	154.2
0.7–1.0	$0.70^{+0.33}_{-0.34}$	$0.98^{+0.28}_{-0.27}$	0.26 (3)	273.7